Chapter 6

DISCUSSION

6.1 Pressure Dependence of Elastic Properties

As outlined in Chapter 1.2 the seismic velocity of a rock depends on a number of *intrinsic* (such as the elastic constants of the rock-constituting minerals and matrix structure) and *extrinsic* parameters (e.g. volume and geometry of pore space, and pore fillings) [e.g. Christensen, 1966; Kern, 1982; Mainprice & Humbert, 1994; Wyllie et al., 1956; Nafe & Drake, 1957]. These parameters depend in turn on pressure P as well as temperature T, whereby P and T have an opposite effect. Generally, the positive dependency of elastic moduli on pressure results in an intrinsic increase of velocities with increasing pressure. However, at low confining pressures the velocity–pressure relation is dominated by variations in the pore structure of the rock. Increasing the confining pressure leads to a successive reduction of pore space between 0.1 and 200 MPa and an enhancement of grain contacts, which is assumed to be the main factor for the sharp increase of velocities at low confining pressure [e.g. Birch, 1960, 1961; Simmons, 1964a]. The reduction of pore space is highly efficient for cracks and pores with low aspect ratios ($\alpha < 0.01$), because thin, flat cracks, previously defined as *soft* or *compliant porosity*, are very sensitive to stresses normal to the crack [see Walsh, 1965; Mavko & Jizba, 1991; Shapiro, 2003]. In contrast, spheroidal pores ($\alpha > 0.1$ - *stiff porosity*) may remain open to a certain extent even at pressures of 1 GPa, but are assumed to have a minor influence on the linear part of the velocity–pressure relation, which is regarded to represent an intrinsic behaviour above 200 MPa [e.g. Birch, 1960; Simmons, 1964a; Christensen, 1965]. In fact, this seems to apply only for low porosity rocks (crystalline rocks), while in porous rocks (e.g. sandstones) changes in the elastic moduli and velocities are controlled over the whole pressure range predominantly by the pressure dependence of the porosity [Shapiro, 2003].

Rock	Modal Analysis [%]	p Derivates [km s^{-1} MPa^{-1}] $\partial v_p/\partial P \times 10^{-4}$	$\partial v_s/\partial P \times 10^{-4}$	T Derivates [km s^{-1} °C] $\partial v_p/\partial T \times 10^{-3}$	$\partial v_s/\partial T \times 10^{-3}$	System	Ref.
Amph.	55 am, 40 plg, 5 en	—	—	-0.55*	—	drained	[1]
Amph.	45 am, 43 plg, 3 mi	0.36	0.17	-0.24	-0.21	drained	[2]
Amph.	72 am, 24 plg, 3 qz, 1 grn	0.66	0.28	-0.07	-0.14	drained	[2]
Amph.	72 am, 12 plg, 10 epi	0.28	0.13	-0.17	-0.20	drained	[2]
Amph.	48 am, 18 plg, 27 qz, 4 epi	0.23	0.09	-0.10	-0.18	drained	[2]
Amph.	—	—	—	-0.13	-0.17	drained	[3]
Amph.	—	—	—	-0.71	-0.18	drained	[3]
Amph.	—	0.28	0.20	-0.38	-0.22	drained	[5]
Amph.	63 am, 35 plg, 2 bt	0.57	0.20	-0.23	-0.19	drained	[7]
Amph.	26 am, 55 plg, 18 bt, 1 epi	0.46	0.16	-0.27	-0.15	drained	[7]
Amph.	—	—	—	-0.47	—	—	[8]
Amph.	34 am, 61 plg, 3 epi, 2 pump	0.43	—	-1.33$^{\diamond}$	—	undrained	[*this study*]
Anorth.	5 am, 70 plg, 2 bt, 15 opaq, 7 hyp	—	—	-0.41	—	drained	[1]
Serp.	—	—	—	-0.13	-0.17	drained	[4]
Serp.	98 chry + liz	—	—	-0.68*	—	drained	[1]
Serp.	78 ant, 28 ol, 2 opaq	—	—	-0.92*	-0.54*	drained	[4]
Serp.	74.9 ant, 20.3 ol, 3.8 ox 1.0 others	0.57	0.01	-0.38	-0.41	open	[6]
Serp.	30 ant, 60 ol, en opaq	0.64	0.27	-0.60$^{\bullet}$	-0.46$^{\bullet}$	undrained	[*this study*]

am=amphibole, ant=antigorite, bt=biotite, chry=chrysolite en=enstatite, epi=epidote, grn=garnet, hyp=hyperstene, liz=lizardite, mi=mica, ol=olivine, opaq=opaquos, ox=oxides, plg=plagioclase, pump=pumpellyite, qz=quartz

**: $(\partial v_{p,s}/\partial T)_P$ refers to 200 MPa confining pressure (P_c); $^{\diamond}$: P_c = 800 MPa; $^{\bullet}$: P_c = 900 MPa; without mark: 600 MPa.*

[1]= Christensen, 1979; [2]= Kern & Richter, 1981; [3]= Kern, 1982, [4]= Popp & Kern, 1993; [5]= Ito & Tatsumi, 1995; [6]= Kern et al., 1997; [7]= Kern et al., 1999; [8]= Aizawa et al., 2002

Table 6.1: *Compilation of pressure and temperature derivatives of P and S waves of amphibolite, anorthosite, and serpentinite samples from the literature and this study. The experiments referred to in the literature were performed in* **drained** *systems, where the water can be released during the heating. In contrast, the experiments described in this study were conducted in an encapsulated system, where water remains in the sample (***undrained***).*

6.1.1 Chephren Amphibolite

The experimental results of the Chephren amphibolite obtained in this study are generally consistent with the literature data and the established interpretations. The highest *non-linear* increases in velocity between 0.1 and 200 MPa were observed for the samples with the highest initial porosity, CH_{E_1} and CH_A, whereby the latter was characterised by an initial open porosity of 0.24 % before the experiment, which was restricted to flat cracks with low aspect ratios exclusively (Fig. 4.6 b). For sample CH_{E_1} an open porosity of about 0.005 % was determined before the first pressure experiment, which ended with the before mentioned *blow-out*. It must be assumed that the sample was modified by mechanical cracking as a result of the *blow-out*, clearly shown by the much lower velocity at ambient conditions, in comparison to other pre-run samples. However, the new "initial" porosity was not quantified to avoid a further damage of the complex set-up. The progressive closing of these additional artificial cracks is displayed by the strong non-linear increase of velocity at pressures below 200 MPa in the second pressure run (Fig. 6.1 black data set).

In the presented experiments, the deviations from the linear velocity–pressure relation within the first 200 MPa are smaller for lower porosity values determined for the samples (Fig. 5.1). The deviation tends to almost zero for sample CH_{E_2}, which may reflect the very low initial porosity of 0.012 % (Fig. 6.1 blue data set). This behaviour was not described before in the literature, possibly because a standard preparation procedure is the drying of ultrasonic samples at temperatures $\geq$ 100 °C to reduce the moisture in the pore space. This can lead to the formation of cracks due to inhomogeneous and anisotropic thermal expansion of the rock-forming minerals (thermally induced cracks) and the high thermal expansion of boiling water. In this study, this effect is lowered by drying the samples at only 60 °C in a vacuum-oven. P wave pressure derivatives of 0.36 $\times 10^{-4}$ to 0.61 $\times 10^{-4}$ $[km\ s^{-1}MPa^{-1}]$ determined parallelly and perpendicularly to the foliation of the Chephren amphibolite, agree quite well with the data published previously (Tab. 6.1 and references in it). The maximum (// lineation) and minimum ($\perp$ foliation) P wave velocities of the foliated Chephren amphibolite at ambient conditions were derived from linear regression of the experimental data above 200 MPa and are compared with those calculated from petrofabric analysis (see Chapter 4.2.2), whereby the latter refer to an idealised pore- and crack-free sample at ambient conditions. From several ultrasonic measurements normal to the foliation a mean $v_{p_{min}}$ of 6.51 km/s was obtained. The mean $v_{p_{max}}$ was found to be 6.84 km/s parallel to the foliation. From single crystal orientation data a $v_{p_{min}}$ of 6.59 km/s and a $v_{p_{max}}$ of 6.95 km/s were calculated (Fig. 6.1). For details of the calculation procedure see Chapter 4.1.2. The discrepancies of the results obtained experimentally and by calculation are $\sim$ 1 % for $v_{p_{min}}$ and $\sim$ 2 % for $v_{p_{max}}$. These are remarkably lower than most values given in the literature so far [e.g. Barruol & Kern, 1996], which show discrepancies of about $\pm$ 5 %. This might be attributed to the fact that the Chephren amphibolite is almost a two-component rock, consisting mainly of plagioclase and amphibole (see Chapter 4). Thus, only two constituents have to be

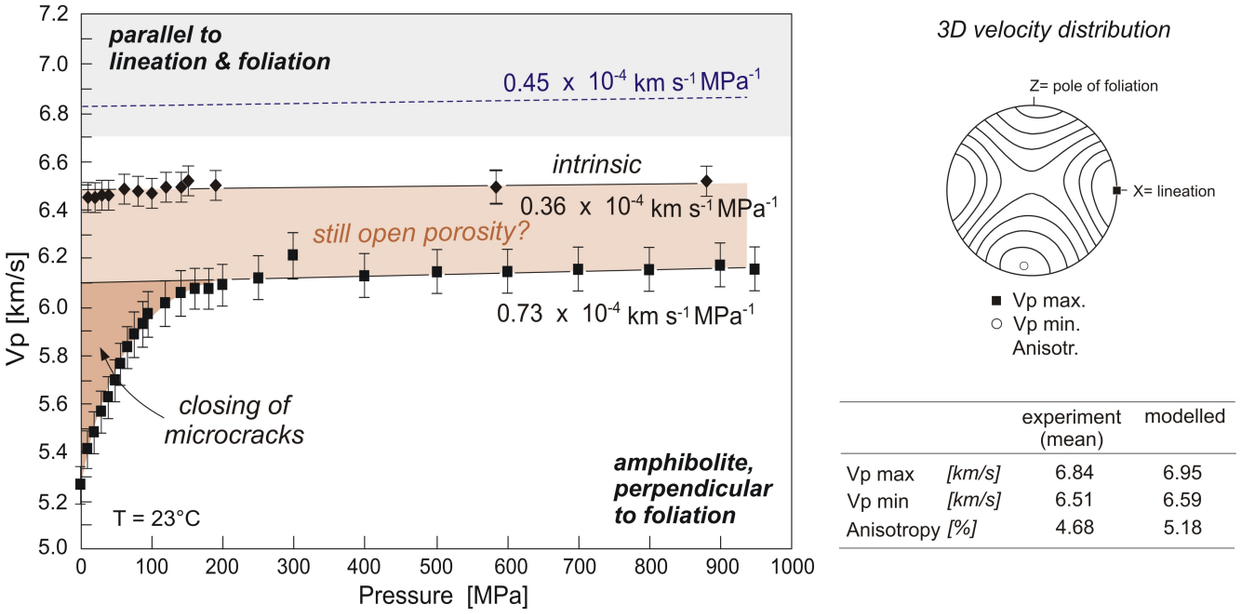

		experiment (mean)	modelled
Vp max	*[km/s]*	6.84	6.95
Vp min	*[km/s]*	6.51	6.59
Anisotropy	*[%]*	4.68	5.18

Figure 6.1: *P wave velocities vs. pressure. The datasets represent the "blow-out" sample (black) and a sample with 0.012 % initial open porosity (blue), both measured perpendicular to the foliation. For the "blow-out" sample an enhanced porosity is assumed.*

taken into account in the velocity calculation from LPO's. As for each mineral phase, the density must be estimated, the error in the calculated velocity might become higher the more mineral phases have to be regarded in a polymineralic aggregate. Furthermore, the medium grain size and the minor alteration of the Chephren amphibolite allows for a grain by grain analysis of the thin-sections to determine LPO's, which are representative for the whole sample. This may result in lower inaccuracies in the single crystal elastic constants compared to investigations on altered samples or samples with heterogeneous grain sizes.

Another aspect might be the generally very low porosity of the Chephren amphibolite, which is developed predominantly as *soft* crack porosity. As a counter-example, P wave velocities derived from the *blow-out* sample are generally significantly lower than those of all other samples investigated normal to the foliation. In this case a $v_{p_{min}}$ of 6.10 km/s was obtained experimentally, which is about 7.5 % lower than the calculated minimum velocity. It is therefore conceivable that the *blow-out* sample exhibit a sustained disruption of the grain structure and an additional *stiff* porosity was developed. This example impressively shows that the linear increase of the velocity-pressure relation at pressure $>$ 200 *MPa* reflects the intrinsic elastic properties of a rock only to a first approximation. Obviously, the influence of the pore space on the velocities is reduced with increasing pressure. Nonetheless, the difference in the pressure derivatives of the *blow-out* sample and the samples, characterised by a minor porosity, is almost 100 %, which is expected if the porosity still dominates the elastic properties of the rock even at

elevated confining pressure [e.g. Shapiro, 2003]. Only if the total porosity is present as crack-porosity or loose grain contacts and thus completely closed at 200 MPa, the measured velocities at $P > 200\ MPa$ may correspond to those in a compact polycrystalline aggregate.

The additional measurement of shear wave traveltimes is very helpful in determining mechanical rock properties. In contrast to the P wave velocities the strong increase of v_s between 0.1 and 150 MPa is rather linear (Fig. 5.3). This results in a v_p/v_s ratio, which is characterised by a pronounced increase between 0.1 and 40 MPa, followed by a rapid decrease. It was already mentioned that the quality of S wave data is low, which makes an interpretation more speculative. There are two possibilities to explain this discontinuous v_p/v_s trend: First, v_s was not determined correctly as the onset of the S phase might be too diffuse to pick traveltimes precisely and v_p/v_s is afflicted by a considerable analytical error. Or secondly, v_s is reliable and changes in the v_p/v_s trend reflect microstructural changes of the sample in combination with changes in the degree of saturation of voids. Assuming residual water in the pore space, the increase of the pressure may elevate the water-saturation in the initially (between 0.1 and 40 MPa) reduced pores space. – It was shown previously [Nur & Simmons, 1969; Nur, 1972] that v_p/v_s increases with increasing confining pressure as v_p and v_s increase due to the gradual reduction of pore volume. As water has a higher compressibility than air, the presence of water in the pore space tends to increase the effective bulk modulus of low porous rocks significantly and consequently, v_p in a saturated rock is higher than v_p in the same but dry rock, whereas v_s remains essentially unaffected. With increasing confining pressure v_p/v_s of the water-saturated rock decreases as water-filled pores tend to remain open due to the rising pore pressure.
For S wave velocities no pressure derivatives were obtained, because in the usable data sets the velocity decreases at pressures higher than 500 MPa (see Chapter 5.1/ Fig. 5.3), which is interpreted as an artefact due to insufficient stress equilibration of the sample.

6.1.2 Malenco Serpentinite

One pressure experiment was conducted on the Malenco serpentinite. Equivalent to the interpretation of the amphibolite data, the strong non-linear increase in P and S wave velocities between 0.1 and 200 MPa (Fig. 5.8 c) is related to the progressive enhancement of grain contacts due to the closure of pores, which again were identified in thin-sections as fine cracks (Fig. 4.11 b). The pressure derivatives obtained from Malenco serpentinite are 0.64 $\times 10^{-4}$ $[km\ s^{-1}MPa^{-1}]$ for v_p and 0.27 $\times 10^{-4}$ $[km\ s^{-1}MPa^{-1}]$ for v_s. Hardly any pressure derivatives are published for serpentinites or serpentinised peridotites. Nonetheless, one v_p-pressure derivative of 0.57 $\times 10^{-4}$ $[km\ s^{-1}MPa^{-1}]$ was found in the literature [Kern et al., 1997], which is in a good agreement with the data presented here.

6.2 Temperature Dependence of Elastic Properties

The increase in temperature lowers the elastic moduli of the rock-forming minerals and in consequence the intrinsic seismic velocity of a rock decreases. Is the heating carried out under a high confining pressure, the influence of microstructural changes on the elastic wave velocities – namely the development of thermally induced microcracks due to different thermal expansion coefficients of the rock-forming minerals – is usually neglected and the velocity–temperature relation reflects, to a first approximation, an intrinsic elastic behaviour of the investigated material [e.g. Christensen, 1979; Kern, 1982]. Next to thermal stress, pore fluids are considered to modify the void space [e.g. Kern, 1982; Popp & Kern, 1993; Ko et al., 1997]. However, temperature derivatives available in the literature refer mainly to measurements conducted under drained conditions. Some of these experiments were performed on encapsulated samples too, but those samples were wrapped with a wire gauze or connected to any other kind of drainage system. Thus, water released during heating was most probably expelled from the samples, preventing the development of an enhanced pore pressure. For drained amphibolites at a confining pressure of 600 MPa, $(\partial \mathrm{v}/\partial T)_{P_c}$ vary between -0.07 and -0.47 $\times 10^{-3}$ $[km\ s^{-1}\ °C^{-1}]$ for P waves and -0.14 and -0.22 $\times 10^{-3}$ $[km\ s^{-1}\ °C^{-1}]$ for S waves, determined in a temperature range between 23 and 500 °C (Tab. 6.1). For Serpentinites temperature derivatives of -0.13 to -0.92 and -0.17 to 0.54 $\times 10^{-3}$ $[km\ s^{-1}\ °C^{-1}]$ are published for P and S wave velocities, respectively, whereby the lower values were deduced between 23 and 600 °C at $P_c = 600\ MPa$. The higher values refer to $P_c = 200\ MPa$ and were determined between 23 and 200 °C. Any variations in this behaviour, such as non-linearity of the velocity–temperature relation or high negative values of $(\partial \mathrm{v}/\partial T)_{P_c}$, are assumed to be related to changes in the microstructure of the sample, as the reconstruction of pore space has a considerably higher effect on velocities than the intrinsic elastic properties of the rock-forming minerals [Christensen, 1979; Ramananantoandro & Manghnani, 1978; Kern, 1978; Lebedev et al., 1991, 1996; Zharikov et al., 1993].

6.2.1 Chephren Amphibolite

In the Chephren amphibolite, essentially five water-containing phases are relevant as fluid sources: amphibole and accessory muscovite, pumpellyite, chlorite, and epidote. At equilibrium conditions these minerals dehydrate at a confining pressure of 800 MPa at about 900, 350, 400, and 600 °C, respectively (Fig. 6.2) [Gottschalk, 1997]. In the course of water release and trapping inside the undrained sample, the pore pressure should increase and dilate grain bounderies as the effective pressure is reduced ($P_{eff} = P_c - n\,P_{fl}$; Eq. 1.9). This in turn, should result in a drop of velocities. When the kinetics of mineral reactions are taken into account, the first variation from the intrinsic velocity–temperature relation

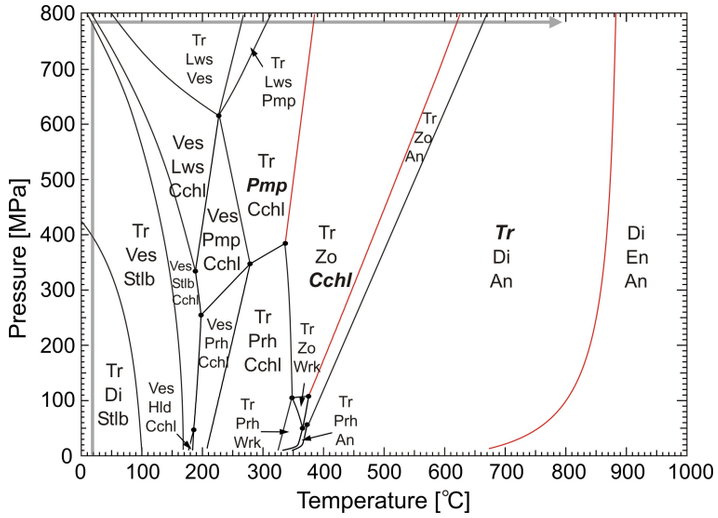

Figure 6.2: *From phase diagram dehydration temperatures of 400 °C for pumpellyite* (**Pmp**)*, 600 °C for chlorite* (**Cchl**)*, and 900 °C for amphibole* (**Tr**) *at 800 MPa can be deduced [after Gottschalk, 1997]. The grey arrow marks the path the samples followed during the experiment.*

is expected at about 500 °C for the muscovite and pumpellyite decomposition, which refers to an overstepping by about 100 K. Furthermore, it was expected that the degree of velocity reduction correlates positively with the amount of water, expelled from hydrous minerals, especially under a high confining pressure. In the case of Chephren amphibolite, only the minor and accessory phases muscovite, pumpellyite, and chlorite release water in the considered temperature range of 23 to 750 °C. Moreover, thermogravimetric measurements revealed a general OH-deficit of the Chephren amphibolite. Consequently, it was expected that the decrease in velocity is remarkably lower for the amphibolite than for the serpentinite.

Nonetheless, the velocity of the Chephren amphibolite shows a stronger dependence on temperature than the serpentinite. The velocity–temperature relation displays four general stages (Fig. 6.3), which are interpreted as: **(1)** dilation of pores due to thermal expansion of fluids trapped in isolated pores, **(2)** hydrofracturing and, consequently, fluid expulsion and compaction of pores, **(3)** dehydration of minor and accessory mineral phases (muscovite, pumpellyite, chlorite) and repeated increase of the pore-fluid pressure in a discontinuous pore network, and **(4)** anew pore pressure excess, resulting again in the development of an interconnected pore network, the expulsion of fluid, and pore compaction.

In **stage 1**, already in the low temperature range between 23 and $\sim$ 400 °C and far below the expected dehydration conditions of the hydrous phases the velocity decreases by about 6 to 10 %, and thus deviates significantly from most literature data [e.g. Christensen, 1979; Kern et al., 1997]. Previous studies on drained amphibolite samples found only a slight linear decrease of velocity up to 500 °C with a gradient of -0.10 $\times 10^{-3}$ to -0.47 $\times 10^{-3}$ $[km\ s^{-1}\ °C^{-1}]$ (Tab. 6.1 and references in it), which is attributed to

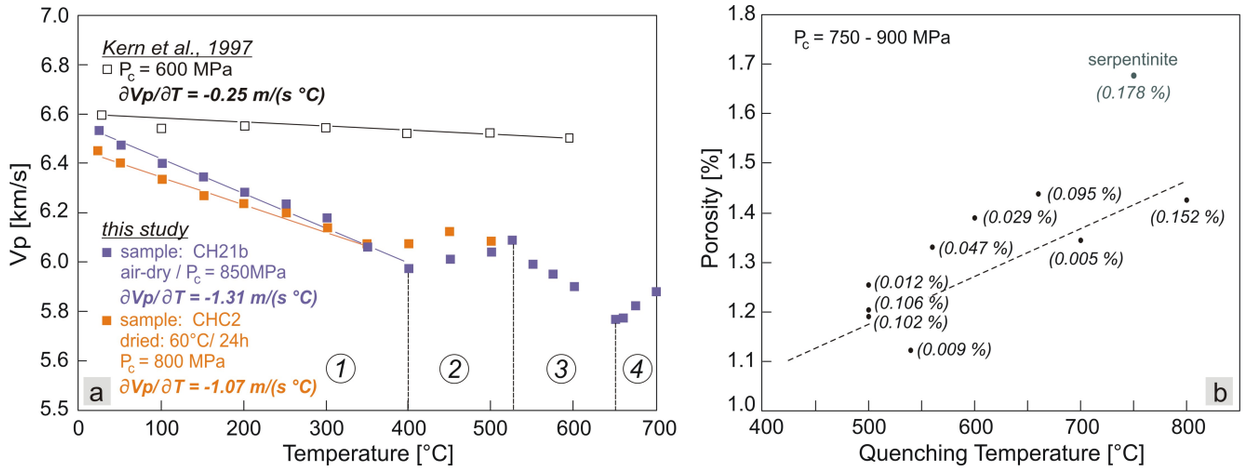

Figure 6.3: *(a) P wave velocities vs. temperature - a comparison of undrained Chephren amphibolite (air-dry and oven-dry) and an amphibolite sample measured at drained conditions [Kern et al., 1997]. The numbers in circles refer to different stages of the $v_p - T$-trend and are explained in the text. (b) The porosity of amphibolite and the serpentinite samples after the experiment vs. quenching temperatures. The numbers in brackets refer to the initial porosity. The general trend displays a slightly higher porosity with increasing temperature.*

changing elastic constants of the rock-forming minerals with increasing temperature.

The results obtained in this study, however, do not support an interpretation in terms of temperature induced changes in single crystal elastic properties and hence intrinsic velocity changes. An extensive reduction of the velocity rather argues for a general disruption of the rock‘s microstructure and the opening of flat cracks in particular, as essentially a small apect ratio strongly affects the elastic properties [Walsh, 1965; O‘Connell & Budiansky, 1974]. And indeed, the value of the open porosity increases from less than 0.15 % in the starting material to about 1.5 % after the samples were exposed to 650 to 700 °C (Fig. 6.3 b). Microstructural analyses on quenched samples reveal fairly well developed fracture frameworks, which are linked primarily to the grain boundaries and the cleavage planes of the minerals and possess therefore low aspect ratios (Figs. 4.6 c and d). It cannot be decided, in how far the microcracking developed due to the quenching and/ or the pressure release after the experiment. However, regarding the results obtained *in-situ* in this study, microcracking in the course of the temperature run has to be taken into account. Possible mechanisms are *thermally induced microcracking* due to different thermal expansion coefficients of the rock-constituting minerals, and *variations of the pore-fluid pressure* in a solid–fluid system due to mineral decomposition and the release of structurally bonded water and the higher volumetric expansion of fluids by heating compared to minerals.

Kern [1978] recommended a value of 1 MPa/ K to suppress *thermally induced microcracking*. In the presented study, the confining pressure is 750 to 900 MPa and thus at least 150 MPa higher than for the reference data in Tab. 6.1. Ramananantoandro & Manghnani [1978] argue, however, that internal

stresses in their encapsulated samples due to anisotropic thermal expansion of constituent mineral grains can cause crack-formation even at 1 GPa gas-pressure. The resulting discrepancy between $(\partial \mathrm{v}_p/\partial T)_{P_c}$ from single crystal data (-0.44 $\times 10^{-3}$ $[km\ s^{-1}\ °C^{-1}]$) and their experimental measurements (-0.67 $\times 10^{-3}$ $[km\,s^{-1}\,°C^{-1}]$) may be one explanation for the broad spectrum of published velocity–temperature derivatives. However, *thermally induced microcracking* is regarded not to be the vital mechanism controlling $(\partial \mathrm{v}_p/\partial T)_{P_c}$ in this study, because here the values deviate by up to an order of magnitude from reference data.

On the other hand, the tempering of the samples just before the experiment seems to be a suitable mechanism to control the degree of velocity reduction. Experiments with dried samples (T = 60 and 120 °C) exhibit a reduced decrease of velocity with increasing drying temperatures. The total weight loss of the sample cores by drying is 0.20 to 0.35 mg, which correspond to 0.04 to 0.07 wt%. Other contributions of molecular water, such as fluid inclusions in minerals, are regarded to play a secondary role in the temperature range $<$ 400 °C, as they have predominantly high aspect ratios and thus affect the velocities only minor. The difference between the blue and the red dataset in Fig. 6.3 can be attributed to about 0.1 wt% water trapped inside the encapsulated system. The difference between the intrinsic velocity change of a drained system [Kern et al., 1997] and the velocities determined under undrained conditions in this study are assumed to be caused by $<$ 0.5 wt% H_2O (estimation on the basis of the loss on ignition (Chapter 4)), adsorbed to electrically charged mineral surfaces. As the thermal expansion coefficient of water is an order of magnitude higher than that of solids, an enhanced pore-fluid pressure will result from heating during the experiment and is most probable the main cause for a re-opening of pre-existing microcracks (Eq. 1.9) and the development of new ones supported by a minor amount through thermally induced cracking, even under a high confining pressure.

The introduction of fluid traps into the set-up leads to no deviation in the slope of declining velocities. This might be due to the limited drainage area, as the fluid traps were arranged at the margins of sample and buffer rods to ensure a rather undisturbed transmission of ultrasonic signals (Fig. 5.6). Another possible explanation is an insufficient connecticity of the fluids. The increase of confining pressure during the pressure run possibly pushes the fluids into more or less isolated voids, which dilate and expand with increasing temperature due to an increasing pore-fluid pressure, but form a discontinuous pore space. – From energetic considerations the fluid distribution in polycrystalline aggregates is linked to the dihedral angle θ between two crystal faces: To minimise the surface energy isolated pores exhibit high aspect ratios and form preferentially at grain corners with θ $>$ 60 °C and a high pore aspect ratio, while for θ $<$ 60 °C the interconnection of the fluid along grain edges is energetically favored [Smith, 1964; Bulau & Waff, 1979; von Bargen & Waff, 1986; Watson & Brenan, 1987]. Although in *stage 1* the porosity is assumed to be isolated, a predominant concentration of fluids in triple junctions is excluded here as these high aspect ratio–pores should affect the elastic wave velocities of a sample only minor. As suggested schematically in Fig. 6.5 a the low aspect ratio, disk-shape distribution of the fluid between two grain

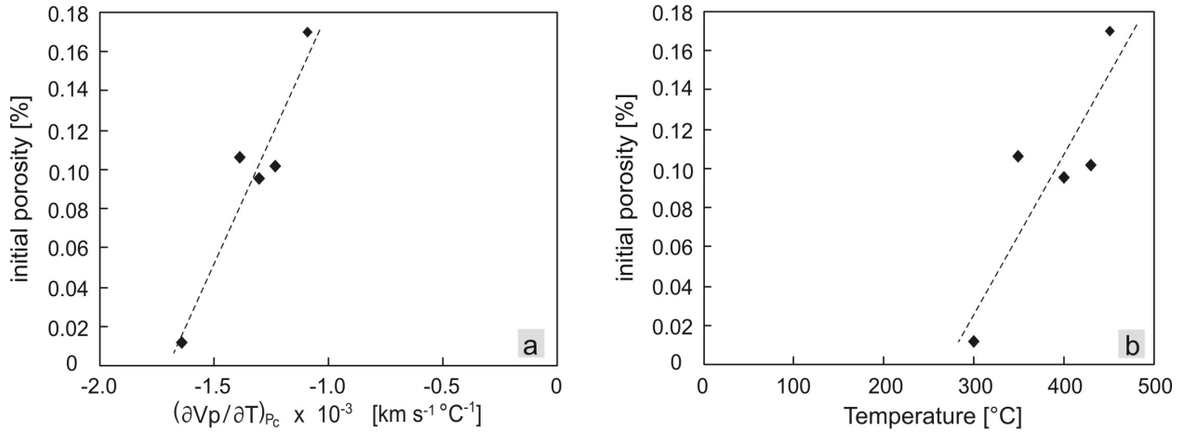

Figure 6.4: *Initial porosity vs.* $(\partial v_p/\partial T)_{P_c}$ *of air-dry amphibolite samples (a) and the temperature* T_c *at which the reversion of the* $v_p - T$*-trend is observed (b).* $(\partial v_p/\partial T)_{P_c}$ *was determined between 23 °C and* T_c*. Both the slope and* T_c *seem to depend on the initial porosity of the samples.*

faces and along cracks is more suitable to explain the reduction of P wave velocities by up to 9 % during the first dilatational phase and confirm previous observations on the distribution of low melt fractions in upper mantle rocks [Faul, 1997].

The lower the initial porosity of the sample was, the more effective seemed to be the pore dilation, which is displayed by a more pronounced reduction of v_p (Fig. 6.4 a). If the dilation of the pore space is insufficient to provide further expansion of the pore fluid, a pore pressure excess develops, which was reached at lower temperatures the lower the initial porosity of the sample was (Fig. 6.4 b) [Wong et al., 1997]. To estimate roughly the critical temperature T_c at which P_p and P_c equalise and cancel out P_{eff}, the increase of fluid pressure due to an increase of temperature was calculated for a water-filled inclusion, embedded in an anorthite crystal (Fig. 6.5 b). This model considers the compressibilities and thermal expansion coefficients of both the host crystal and the fluid inclusion [Gottschalk, pers. comm.]. For a confining pressure P_c of 850 MPa the critical temperature T_c is $\sim$ 450 °C, which approximately corresponds to the temperatures at which the reversion of the $v_p - T$-trend was observed. Considering that T_c may be even lower when the fluid is stored in oblate pores with low aspect ratio along grain boundaries, the minimum velocities of *stage 1* (Fig. 6.4 b) may represent nearly zero effective pressure conditions. Accordingly, by the end of *stage 1* the tensile strength of the rock sample is reached and a small fraction of fluid may already expells from the sample, accounting for the onset of a time-variant velocity increase (Fig. 5.7).

At the beginning of **stage 2**, the successive increase of the pore fluid pressure exceedes the tensile strength of the rock (Fig. 6.5 b) and microcracks (hydrofractures) will open abruptly to form an interconnected pore network. The expulsion rate from the sample interior into the capsule reaches a maximum and consequently the pore pressure in the fractures will reduce. Presumably, this results in the subsequent collapse of hydrofractures, and pores and the sample compacts again, which seems to be the

dominating process causing a re-increase of velocities at higher temperatures. Additionally, microstructural analyses of thin-sections of a sample, quenched from this temperature range, reveal, starting from ore grains, the precipitation of hematite along microcracks. Thus, besides the hydrofracture mechanism a partial chemical compaction of the sample by precipitation of a new mineral phase may contribute to the increase of the P wave velocity and provide evidence for a fracture-channeled fluid flow.
Hydrofracturing is an elusive process as the fluid distribution varies on short time scales and changes the seismic response of the sample. In the regarded temperature interval, the time-variant data recording at constant *PT* conditions shows an increase of velocities with increasing duration, which can be attributed to a changing fluid distribution and resulting modifications of the pore structure.

In **stage 3**, the velocity decreases again, indicating a considerable re-increase of the porosity. It is supposed that a discontinuous pore network is present at the beginning of *stage 3* caused by a partial mechanical and chemical compaction in *stage 2*. Temperatures above 500 °C, however, induce the dehydration of pumpellyite, and muscovite and perhaps already start the decomposition of chlorite. Water released by decomposition ingresses into the intergranular space and, equivalent to *stage 1* seems to be stored in the sample and not to be expelled instantaniously. Again, this leads to a progressive increase of pore-fluid pressure and consequently causes the re-opening and formation of microcracks. The slope of the velocity reduction is steeper compared to *stage 1*, which is possibly linked to a pervasive disruption of the sample during the previous hydrofracturing and the easier dilation of these additional cracks.

Stage 4 is assessed as equivalent to *stage 2*. Pore fluids trapped during *stage 3* can not drain away such that the effective confining pressure P_{eff} decreases continuously with increasing temperature due to a successive decomposition of hydrous minerals and/ or thermal expansion of the pore fluid. At $\sim$ 650 °C the P wave velocity increases again, suggesting that a P_{eff} of zero may be reached ($P_{pore} \approx P_c$) and the strength of the sample is exceeded. Consequently, drainage paths evolve again and fluids are readily expelled causing the anew compaction of the sample.

In summary, the temperature experiments on the Chephren amphibolite gave unforeseen but reproducible results, suggesting that the data are representative for this rock sample at *undrained* conditions. The discontinuous velocity–temperature relations indicate a cyclic fluid pressure-controlled reconstruction of the pore and fracture system, which alternates between dilatancy and collapse/ sealing and causes temperature- and time-dependent variations in the sample permeability: The concentration of fluids in isolated voids or discontinuous pore network where high fluid pressures are reached, change with stages where an interconnected pore network develops and fluids can drain from the sample. Initially, pore pressure excess is reached by thermal expansion of small amounts ($\sim$ 0.3 wt% H_2O) of adsorbed (or interlayered) water. The secondary decrease of velocity is attributed then to the dehydration of minor rock-constituents. From modal analysis the amount of water released by mineral decomposition at ex-

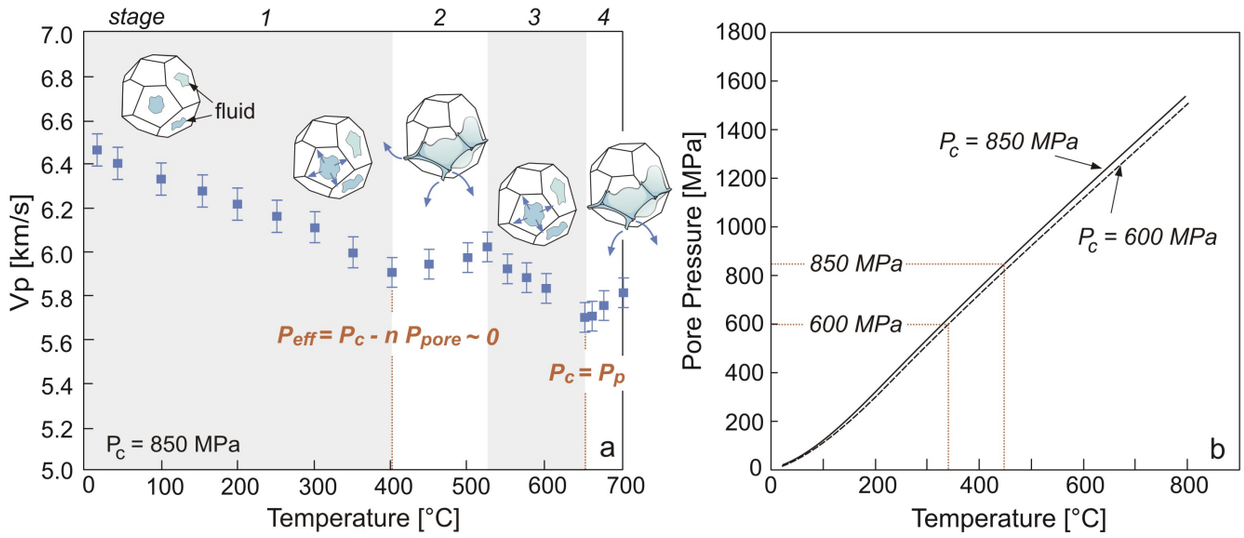

Figure 6.5: *(a) P wave velocity as a function of temperature. The decrease of velocity stops, when the expected fluid pressure in the pores P_p correspond to the confining pressure P_c. It is assumed that isolated pores interconnect after the tensile strength of the rock is exceeded and form a drainage network. (b) Increase of fluid pressure due to an increase of temperature was calculated for a water-filled inclusion, embedded in an anorthite crystal.*

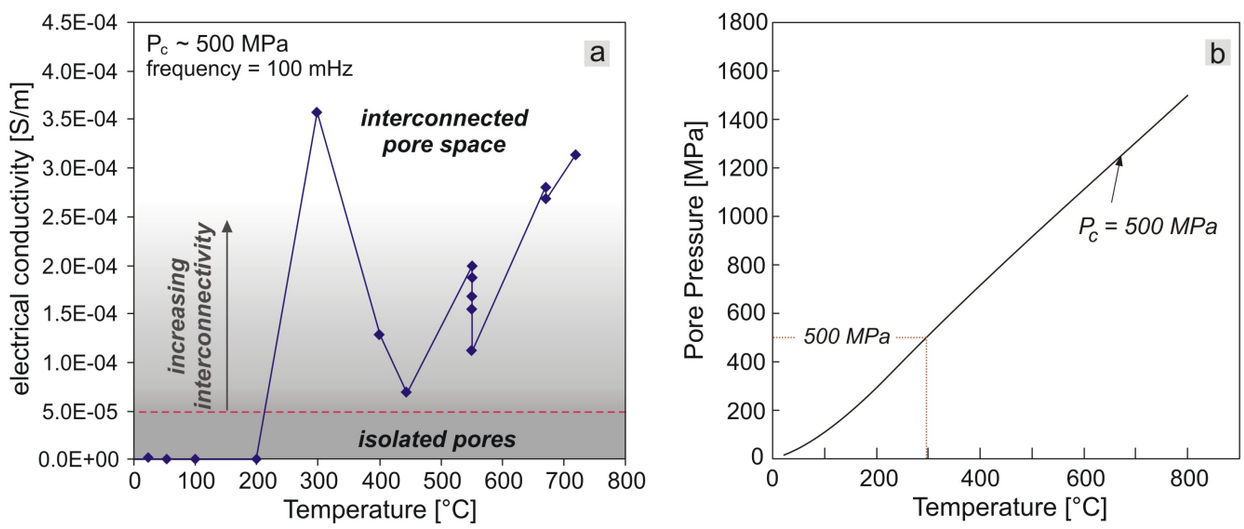

Figure 6.6: *(a) The electrical conductivity was measured on an encapsulated sample of air-dry Chephren amphibolite with a frequency of 100 mHz. With increasing temperature an alternation of the electrical conductivity was observed and may display a temperature dependent pore fluid connectivity varying from isolated or discontinuous interconnected pore fluids (low electrical conductivity) to a continuously interconnected fluid film. (b) For a confining pressure P_c = 500 MPa the zero differential pressure $P_{diff} = P_c - P_{pore}$ is reached at about 300 °C. The calculation is based on the thermal expansion coefficients of anorthite and water considering the compressibility of both materials.*

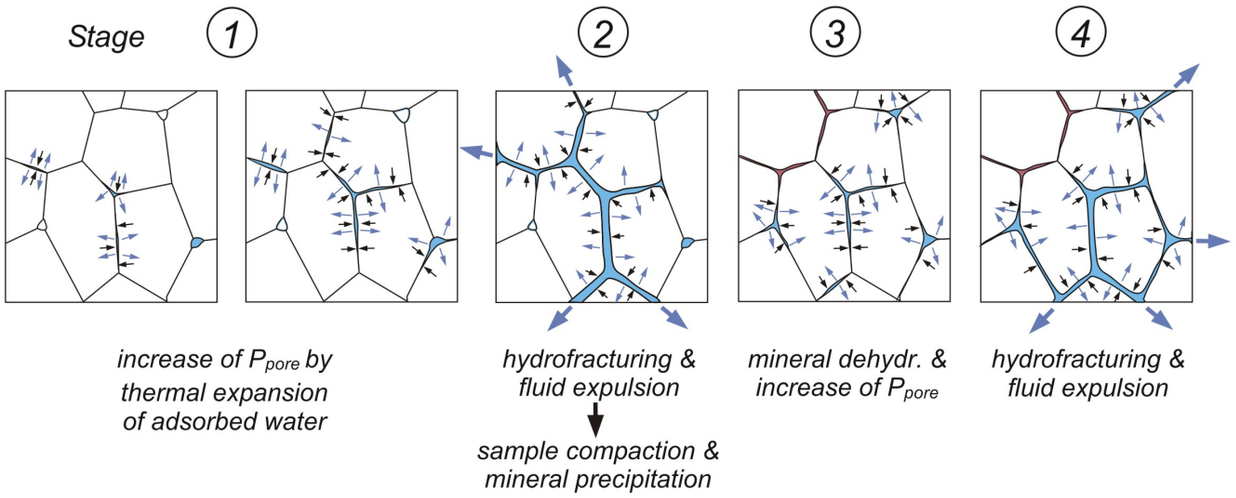

Figure 6.7: *The velocity data indicate a continuous reconstruction of the pore space with increasing temperature. (1) Initially, the interconnectivity of pores and therefore the permeability is expected to be low and a pore pressure is regarded to build up by thermal expansion of residual water on grain boundaries. (2) If the dilation of pore space is insufficient to enable a further expansion the hydrofracturing of the sample promote the expulsion of the fluid, which is linked to a subsequent crack collapse and mineral precipitation. (3) The onset of mineral dehydration increases the pore pressure again and causes (4) a further hydraulic fracturing.*

perimental conditions is maximum 0.2 wt%, assuming that the dehydration of mica, pumpellyite, and chlorite was completed. Measurements perpendicular and parallel to the foliation as well as microstructural analyses of thin-sections point to an isotropic distribution of microcracks, formed predominatly along weak grain boundaries. For the continuation of the dehydration of the amphibolite at temperatures higher than 750 °C rock (decomposition of chlorite, epidote, and amphibole) further sequences of velocity reduction – velocity re-increase are presumed, as the measurement of loss of ignition (Chapter 4) revealed a moderate, continuous release of water with increasing temperature.

Additional support for the concept of periodic pore isolation and pore interconnection is provided by measurements of the electrical conductivity performed on an encapsulated sample of the Chephren amphibolite [Bruhn, pers. comm.]. Fig. 6.6 a displays the change of electrical conductivity as function of temperature. At temperatures between 23 and 200 °C no significant change in electric conductivity was observed, while it increases dramatically between 200 and 300 °C, followed by repeated phases of increasing and decreasing electrical conductivity. The transition between the several phases are linked to critical temperatures, which are considerably lower than those observed in the ultrasonic experiments. This seems to be primarily related to the confining pressure, which is substantially lower in the electrical experiment ($\sim$ 500 MPa). Generally, electrical measurements are sensitive only to interconnected fluid films, while isolated pores have a minor influence on the conductivity behaviour and can not be detected by means of this method. The combination of velocity dataset and electric conductivity data may therefore indicate the interconnection of cracks after successive dilation of isolated voids with increasing pore-pressure and fluid drainage out of the sample.

6.2.2 Malenco Serpentinite

The Malenco serpentinite comprises 39.1 % antigorite and minor amounts of chlorite, both containing $\sim$ 12 wt% structurally bonded H_2O, which is expected to be released at about 500 to 600 °C at 850 MPa (Figs. 6.2 and 6.8 a) [Gottschalk, 1997; Schmitt & Poli 1998; Wunder et al., 2000]. Furthermore, deformation experiments revealed that the strength of drained samples is only slightly affected by the increase of temperature, while undrained samples fail at pore pressure excess due to dehydration reactions [Raleigh & Paterson, 1965; Heard & Ruby, 1966]. In previous laboratory deformation experiments the frictional strength of a serpentinised peridotite is reached at 500 °C at 800 MPa (Fig. 6.8 b) [Murell & Ismail, 1976]. In ultrasonic experiments, such a fluid pressure-induced weakening and embrittlement of the sample should be indicated by a significant reduction of seismic velocities.

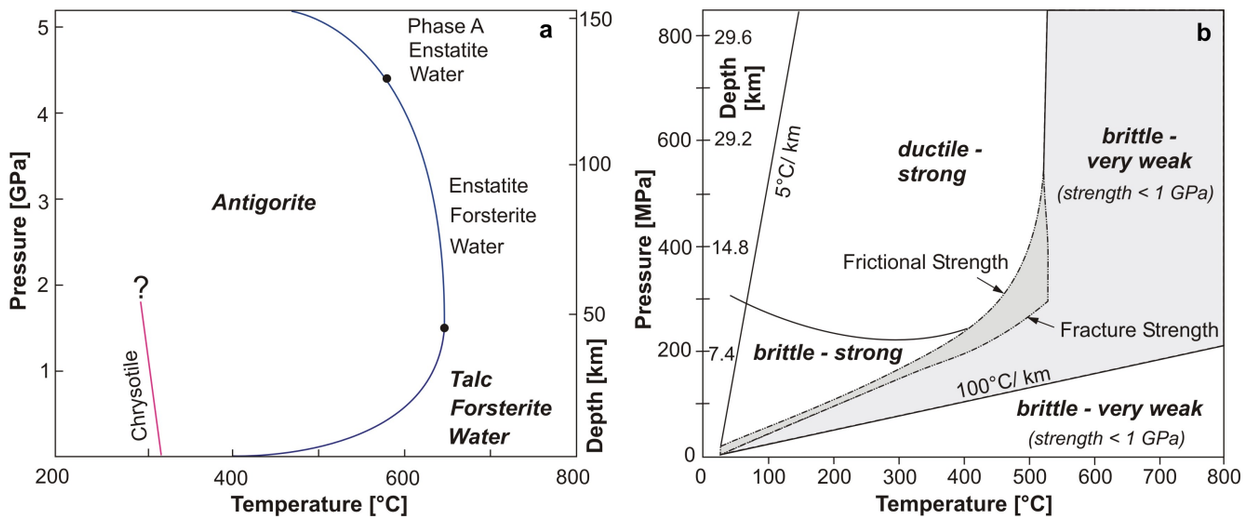

Figure 6.8: *(a) The antigorite decomposition begins at about 600 °C at 850 MPa [after Wunder et al., 2000]. (b) The mechanical behaviour of a partially serpentinised peridotite. The frictional strength of the sample is reached at 500 °C and 800 MPa [after Murell & Ismail, 1976].*

Between 25 and 600 °C the dataset of the undrained Malenco serpentinite (Fig. 6.9) is in good agreement with a dataset derived from a drained serpentinite sample [Kern et al., 1997]. Unlike the effect on the Chephren amphibolite, stored residual water from air humidity apparently has a minor or negligible influence on the seismic velocities of the Malenco serpentinite. The deduced temperature derivatives of $(\partial v_p/\partial T)_{P_c}$ = -0.60 $\times 10^{-3}$ $[km\,s^{-1}\,°C^{-1}]$ and $(\partial v_s/\partial T)_{P_c}$ = -0.46 $\times 10^{-3}$ $[km\,s^{-1}\,°C^{-1}]$ are in the range of intrinsic derivatives deduced for serpentinites so far (Tab. 6.1). Hence, between 23 and $\sim$ 600 °C the velocity–temperature relations are interpreted to reflect in a first approximation an intrinsic reduction of the velocity, due to the temperature dependency of the elastic moduli of the rock matrix.

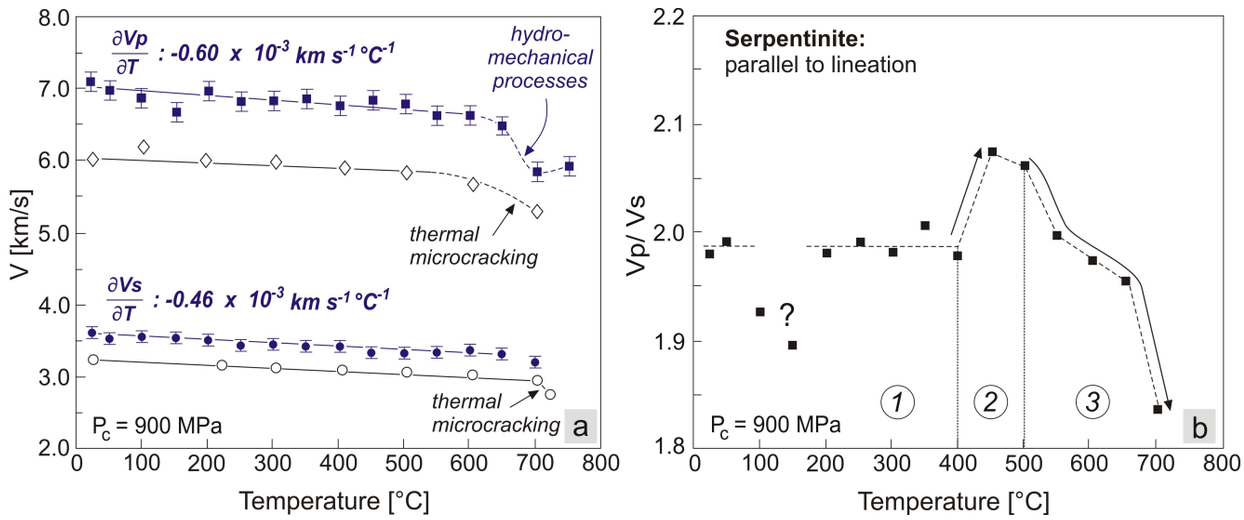

Figure 6.9: *(a) P and S wave velocities of the undrained Malenco serpentinite vs. temperature. For comparison a dataset for a serpentinite, measured under drained conditions by Kern et al. [1997], is plotted (open symbols). (b) v_p/v_s as function of the temperature. Three different stages are resolved. See text for explanation.*

Nonetheless, in ignition experiments (Chapter 4.2) the Malenco serpentinite lost more water ($\sim$ 0.7 wt%) at temperatures $<$ 150 °C than the Chephren amphibolite. Hence, it is not to be supposed that the serpentinite sample introduces less humidity to the encapsulated system than the amphibolite. Furthermore, the analysis of thinsections of the quenched serpentinite sample reveals a preferred alignment of cracks in the foliation plane. Thus, the formation of microcracks might be not well resolved in the ultrasonic data, because the velocities were determined parallel to the foliation and it is quite conceivable that the decrease in velocity is more pronounced in measurements perpendicular to the foliation plane. Generally, the crack formation in the Malenco serpentinite is less pervasive than in the Chephren amphibolite, possibly because the fine-grained, interlocked minerals of the serpentinite resist the stress produced by thermal expansion of residual water [Robertson, 1955; Brace, 1961; Wang, 1994]. Strength anisotropy due to shape-preferred orientation of the antigorite fibres [Přikryl, 2001] may support the development of fluid channels in the foliation plane and the successive squeezing of fluids out off the sample. This, in turn, should be linked to a successive enhancement of grain contacts, causing an increase of the v_p/v_s ratio with increasing temperatures. However, this interpretation is not supported by the experimental data. The considerable increase of the v_p/v_s ratio between 400 and 500 °C from a mean value of 1.98 by $\sim$ 4% is caused by a slight increase of the compressional wave velocity at the concurrent decrease of the shear wave velocity and rather indicates the widening of pores due to thermal expansion of residual pore water (*stage 2* in Fig. 6.9 b). Hence, the scenario of trapped moisture in isolated pores inside the sample is favoured. At temperatures lower than 400 °C the water is regarded to be stored in fluid pockets in triple junctions or resides in isolated, low aspect ratio inclusions in the foliation plane. Thus it influ-

ences the elastic properties measured parallel to the foliation of the sample only minor. Nonetheless, the present data are not sufficient for a final evaluation of the fluid distribution in the sample at temperatures below 600 °C. Similar to the Chephren amphibolite, the investigation of the Malenco serpentinite has to be supplemented by measurements normal to the foliation, by a time-variant data recording and possibly by measurements of the electrical conductivity.

At temperatures above 600 °C the velocities in a drained [Kern et al., 1997] as well as in the undrained sample [this study] decrease substantially (Fig. 6.9). But while the velocity reduction in the reference dataset reflects a thermally induced microcracking due to a lower confining pressure (600 MPa), under undrained conditions at higher confining pressure (900 MPa) the pore-fluid pressure is assumed to increase either by further thermal expansion of the residual water or by the initiation of dehydration of antigorite and the minor phase chlorite. Possibly both processes contribute to a hydromechanical reconfiguration of the void structure (formation and dilation of cracks/ Fig. 4.11 b – d and Fig. 6.3 b) and the sharp velocity reduction in the Malenco serpentinite at temperature higher than 600 °C. The dramatic decrease of v_p/v_s (*stage 3* in Fig. 6.9 b) already starts at $\sim$ 500 °C and possibly indicates an upcoming hydrofracturing event.

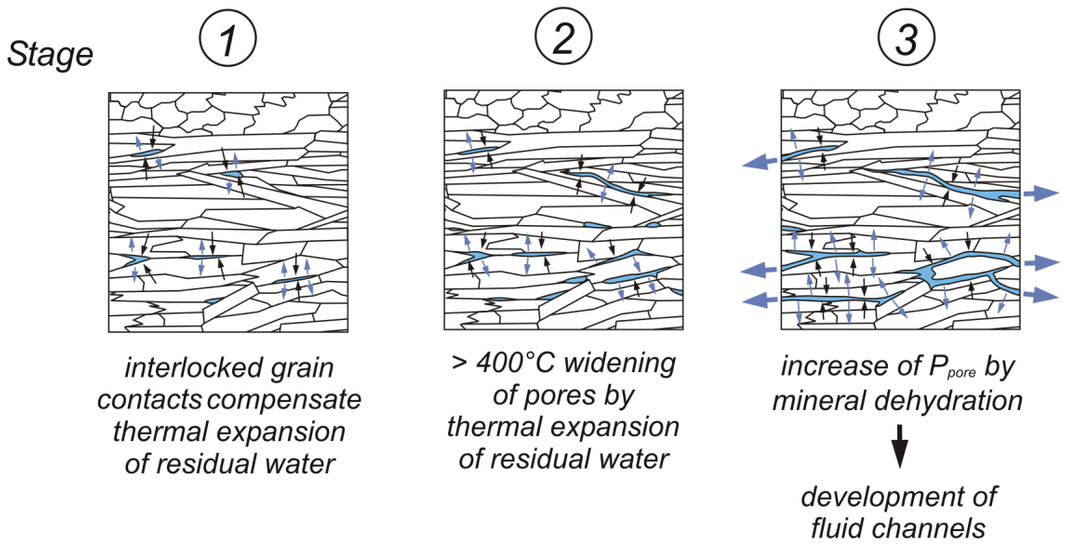

Figure 6.10: *Similar to the Chephren amphibolite residual water is trapped insight the serpentinite sample. However, the fine-grained, interlocked minerals of the serpentinite compensate the stress produced by thermal expansion of the fluid on the grain boundaries (*stage 1*) until temperatures of 400 °C are reached (*stage 2*). The release of larger quantities of water by mineral dehydration and the further thermal expansion of the residual fluid contribute to the development of fluid channels in the foliation plane (*stage 3*). The numbers in circles refer to stages marked in Fig. 6.9*

6.3 Conclusion

Air-dry, low-porosity samples of both the Chephren amphibolite and the Malenco serpentinite were investigated at similar experimental conditions. On both samples an increase of porosity by a factor of 10 to 15 was observed after the experiment. In thinsections, the amphibolite as well as the serpentinite exhibit a slight alteration, indicating a partial dehydration mainly of minor mineral phases. Interlayered or adsorbed water is regarded to be an additional fluid source in both types of encapsulated rock samples. Despite these similarities, however, the processes which modified the Chephren amphibolite and the Malenco serpentinite display remarkable differences in their temperature-dependent elastic behaviours.
Besides the rock composition the most apparent difference in the appearence of the Malenco serpentinite and the Chephren amphibolite is provided by their microstructures, which can contribute to elucidating the variations in the seismic response of both rock samples: The amphibolite is medium grained with straight grain contacts covered with accessory minerals epidote, pumpellyite, and muscovite. Due to heating, the thermal expansion of adsorbed water causes the dilation of cracks and grain contacts. Consequently, for increasing temperatures the velocity decreases more rapidly (by up to 8.5 %) than expected from intrinsic properties. The loss of grain contacts is favoured and amplified by thin films of accessories on the grain boundaries, as in combination with the adsorbed water they form effective lubricants which may enhance the opening of grain boundaries [Isrealachvili et al., 1988; Morrow et al., 2000].
In contrast, the serpentinite is characterised by a fine-grained matrix of interlocked minerals and might therefore have a higher tensile strength. Small amounts of adsorbed water may concentrate in pores. However, as mineral grains are possibly fixed in a more or less rigid position no significant velocity reduction is observed until larger quantities of water are released due to antigorite decomposition, causing a sudden increase of pore-pressure and the abrupt decrease of velocity at 700 °C.
The differences in the elastic behaviour of the Chephren amphibolite and the Malenco serpentinite demonstrate that even at the grain scale in the laboratory the system *rock – supercritical fluid* depends on several concomitant factors, such as textural characteristics (grain size, grain shape, nature of grain contacts), and the quantity and distribution of fluid, which interact in a complex way. Beyond this, the knowledge about the influence of the considered system in terms of *drained* or *undrained* conditions is imperative. From previous studies conducted at lower confining pressures ($\leq$ 600 MPa) it is already known that the release of large quantities of fluids in a narrow temperature window during discontinuous dehydration reactions has an appreciable effect on the porosity and thus the elastic wave velocities even under *drained* conditions [Kern, 1982; Lebedev et al., 1991; Popp, 1994; Ito & Tatsumi, 1995; Lebedev & Kern, 1999], while minor quantities of fluids are expelled from the samples without influencing the elastic properties profoundly. In contrast, the ultrasonic investigations of the Chephren amphibolite reveal that in an *undrained* system there is no implicit need for the sudden release of large amounts of

volatiles to increase the pore-fluid pressure dramatically and ppm amounts of water can be sufficient to induce hydrofracturing processes. The complexity of interactions between these diverse parameters on grain size scale imply the need of further experimental data to approach a deeper understanding of the relationship between the development of a rock–fluid system and the variations of its elastic properties at macroscopic scale. To a first approximation it seems valid to consider *drained* and *undrained* systems to represent end-member scenarios. Processes in geological settings are expected to display a behaviour intermediate between these lower and upper bounds.

6.3.1 Implications for the Interpretation of Seismic Field Data

To interpret seismic field data in terms of lithology and physical state *thermal-petrological-seismological models* are developed [e.g. Hacker et al., 2003a], which usually consider intrinsic velocity-temperature relations, experimentally obtained from investigations of single crystals and drained rocks at high pressure and temperature. The models are based on the assumption of a compact rock matrix and dry grain contacts as in the geological context water loosly-bonded to the rock is expected to be driven off by heat and pressure at greater depth [Morrow et al., 2000; Warner, 2004]. The results of this study highlight, however, that when regarding undrained conditions even for a nominally dry, relatively simple two-component system like the Chephren amphibolite, the relation between velocity and temperature is more complex than considered so far and the influence of microstructural changes due to small amounts of supercritical water in the system cannot be neglected even under high confining pressures. The presented investigations show that < 0.5 wt% water at mechanically weak grain boundaries can decrease the velocity of an initially low-porous rock by up to 9 % and may reduce the velocity-temperature relation by an average factor of 5. This means, in an impermeable rock the increase of porosity due to thermal expansion of moisturised grain contacts has the same effect on elastic wave velocities as the increase of the temperature by factor of 5 at predominance of intrinsic elastic rock properties. Between room temperature and $\sim$ 400 °C the experimentally observed relative velocity reduction for amphibolite is 6 to 9 %. Assuming an intrinsic $(\partial \mathrm{v}_p/\partial T)_{P_c}$, much higher temperatures are required to obtain a comparable velocity reduction. Using an average intrinsic $(\partial \mathrm{v}_p/\partial T)_{P_c}$ value for amphibolite from Tab. 6.1 (-0.28 $\times 10^{-3}$ $[km^{-1}\ °C^{-1}]$), the temperatures are 1400 and 2000 °C, respectively. Still for the highest $(\partial \mathrm{v}_p/\partial T)_{P_c}$ value in Tab. 6.1 (-0.71 $\times 10^{-3}$ $[km\ s^{-1}\ °C^{-1}]$; [Kern, 1982]), temperatures of 550 and 800 °C are needed. Hence, the influence of small amounts of intergranular supercritical fluid on the elastic properties of rocks can outweight that of the temperature.

The interpretation of seismic boundaries in the Earth in terms of changes in lithology, the presence of faults or the presence of water-saturated horizons with high fluid pressure [Etheridge et al., 1984; Pavlenkova, 1988; Nur & Walder, 1990] can be supplemented by the result that velocity contrasts of

several percent can be induced by the presence of small amounts of fluids on mechanically weak grain boundaries. These aspects should be regarded in future models. Above all, more data on the temperature-dependent elastic properties especially of undrained systems are needed to advance the interpretation of geophysical anomalies.

6.3.2 Perspectives

Investigating the influence of supercritical fluids on the elastic properties requires the examination of transient, physically complex processes. This study represents a first approach to determine the elastic properties of an *undrained* rock-fluid system at high confining pressure and temperature ($\leq$ 900 MPa/ 750 °C), and furnishes several potentially promising directions for future ultrasonic experiments at high pressure and temperature:

The variable strength behaviour of the Chephren amphibolite and of the Malenco serpentinite at similar experimental conditions point to the complexity of physical processes in solid-fluid systems. Besides changes in the pore pressure, microstructural characteristics seem to be important concomitant factors controlling the strength of a rock and it is conceivable that for mineralogical similar rocks variations, for instance, in grain size and grain shape may result in a spectrum of various seismic responses. To get a deeper understanding of the interaction between hydrological parameters and rock microstructure and its consequences for the elastic properties of rocks, future studies should concentrate on the investigation of rocks that are chosen specifically for their grain size and the strength of their grain bounderies (interlocked/ non-interlocked).

The dilation of grain contacts and the increase of porosity should increase the attenuation of elastic wave energy. Decreasing amplitudes of ultrasonic signals with increasing temperature as well as temperature-dependent variations in the signal shape observed during this study (Chapter 3) possibly indicate microstructural changes of the sample. However, the utilised set-up allows only a descriptive analysis of the observed phenomenons, and more effort is needed on a quantitative analysis of seismic attenuation.

Ultrasonic measurements of seismic velocities could be supplemented by the determination of the electrical conductivity, which is besides the seismic attenuation a highly sensitive measure of changes in the pore space and fluid distribution of a rock sample.

In some experiments carried out on the Chephren amphibolite in this study traveltime traces recorded in the temperature range between 400 and 450 °C are very noisy and exhibit sporadically signals, which can not be correlated with the input signal. These may indicate acoustic emission signals, which may provide deeper insights in the hydrofracturing of the sample. They could be analysed in more detail by a continuous data aquisition instead of the short discontinuous, stacked time windows recorded in this study.

In both the amphibolite and the serpentinite the extent of dehydration is low as the reached temperatures were not high enough to pass through dehydration reaction completely, and an evaluation of the seismic response at higher temperatures must be undoubtedly speculative. To investigate the influence of the dehydration regime (continuous vs. discontinuous dehydration) on the seismic signature, the temperature range has to be expanded to higher temperatures. This should be possible by a slight reduction of the sample diameter and a further enhancement of the thermal insulation of the furnace. Appropriate changes of the experimental set-up were already carried out and first calibration tests were promising.